Regular Article

Band Gap Engineering of TiO₂ Anatase through Cobalt and Nitrogen Co-doping: A Periodic Hybrid-DFT Study

R. Behjatmanesh-Ardakani[a],* and A. Moradzadeh[b]

[a]Department of Chemical Engineering, Faculty of Engineering, Ardakan University, P. O. Box: 184, Ardakan, Iran
[b]Department of Chemistry, Payame Noor University, P. O. Box: 19395-4697, Tehran, Iran

Nowadays photocatalysts are widely used to degrade industrial and waste by-products. Among different catalysts, anatase is the most applied one due to its abundance and low cost. However, its large band gap (3.2 eV) limits its efficiency. Many metal and non-metal atoms have been used experimentally to reduce the band gap of anatase. In this paper, we tried to use a hybrid periodic density functional theory (DFT) method to model the solid-state phase of anatase photocatalyst and investigate nitrogen and cobalt substitutional doping on the band gap reduction. In addition to the band gap value, the magnetic properties of defected anatases are also studied. Results show that Co-doping by itself reduces the band gap from 3.56 (for pristine anatase) to 2.4 eV. The band gap reduction for (N, Co) dual-doping depends on the relative positions of N and Co to each other. If Co and N are located far from each other, the band gap reduces from 3.56 to 2.5 and 2.0 eV for spin-up and spin-down, respectively. If they are nearest neighbors, the band gap reduces from 3.56 to 3.2 and 2.6 eV for spin-up and spin-down, respectively. It means that if the position of the doped elements is changed by changing a variable such as the synthesis method, the photocatalytic efficiency of the dual-doped anatase is changed. The spin magnetic moments of single and dual-doped anatase are $1\mu_B$ and $2\mu_B$, respectively, which are in line with the experimental data.

Keywords: Band gap engineering, (N, Co) dual-doped TiO₂, Hybrid-DFT

INTRODUCTION

Anatase are used in different industries such as solar cells and pollutant degradation. The main problem of anatase is its large band gap (3.2 eV) which limits its efficiency because only 5% of the solar spectrum can be used by this large band gap [1]. To increase the efficiency, it is tried to reduce the band gap by interstitial and substitutional metal and non-metal ions. Different cations and anions have been used for anatase band gap engineering to increase its photocatalytic efficiency [2]. Recently, in many cases, a cation and an anion are doped simultaneously (co-doped) to enhance the anatase properties. For example, Sun and Searles studied visible absorption for (N, B) co-doped anatase [3]. They showed that

the catalyst has a 2.0 eV of optical band gap due to the electron excitation from the impurity band to the conduction band. Rashid et al. used (N, S) co-doped TiO₂ for the removal of cationic dyes [4]. (N, S) Doping provides new electrostatic binding sites for the dye adsorptions. Geometrical details, density of states, and dielectric functions of (N, S) co-doped rutile were studied by Chen *et al.* [5]. They showed that interstitial co-doping of nitrogen and sulfur atoms exhibits more red-shift of absorption edge compared to the substitutional doping. Their simulated UV-Vis spectra showed that the co-doped rutile has more photocatalytic activity than the pristine one.

Nitrogen is one of the most common non-metal dopants for anatase, and many experimental and theoretical studies have been done for N-doped TiO₂. For example, Chen *et al.* investigated how nitrogen doping promotes the formation of oxygen superoxide radicals on the surface of TiO₂ [6]. In this

*Corresponding author. E-mail: behjatmanesh@ardakan. ac.ir

research, they showed that N-doped TiO_2 is 1.8 times more active than thermal catalysts for toluene oxidation. Carbon nanotube/(N, F) co-doped TiO_2 composite has been used for water decontamination [7]. Wang *et al.* showed that (C, N) co-doped TiO_2 can absorb more visible light for degradation [8]. Theory can provide us with detailed information about the compounds [9,10]. In the field of semiconductors, theoretical efforts have been made to derive detailed electronic information about single and dual-doped TiO_2. For example, a hybrid method of PBE0 has been used to calculate the band gaps of TiO_2 (001) nanotubes [11]. Navarra et al. used DFT for studying ZnO/N-doped TiO_2 heterojunction [12]. Their results showed that there is a minimal band gap due to the interface between ZnO and N-doped TiO_2. This minimal band gap is smaller than the band gaps of the two separated semiconductors. In conjunction with N, first-row transition metal (TM) cations such as Sc [13], V [14], Cr [15], Fe [16], Cu [17], … were used to reduce further the band gap of TiO_2. Almost for all these TM cations (except some cases), theoretical studies have been done to find their electronic structure (see for example, [18-20]). Cobalt is one of the cases with many experimental studies but few theoretical ones. These theoretical studies contain the work of Yang and Zhou about hydrogen spillover barrier energy on cobalt-doped anatase [21], the research of Jensen and Kilin about the charge transfer process for Co-doped anatase [22], Liu *et al.'s* work on the magnetic property of Co-doped rutile [23], Weng *et al.'s* work on the electronic, optical and magnetic properties of Co-doped anatase [24,25], and Janisch's work on the ferromagnetism of Co-doped anatase [26]. All the above theoretical papers discuss about single-doping of Co without co-doping of nitrogen. Meng et al. used DFT+U to investigate (N, M) co-doped TiO_2, with M=Sc, V, Cr, Mn, Fe, Co, Ni, Cu, and Zn [27]. DFT+U is an alternative approach to the hybrid method that opens the gap compared to the band gaps of pure DFT methods. Increasing U_{3d} on transition metals has been shown to monotonically open the gaps of transition metal oxides [28]. The main drawback of the DFT+U method for opening the band gap is using a high value of the U_{3d} parameter for simulating the experimental band gap. Utilizing large values of U_{3d} is typically regarded as an *ad hoc* fitting parameter lacking a physical basis [28]. To offset a small increase in the band gap caused by the low U_{3d} value, researchers employ U_{3p} for oxygen atoms in transition metal oxides [28]. Meng *et al.* in their work used only U_{3d} parameters with very high values (for example, they used $U_{Co} = 10.1$ and $U_{Cr} = 12$ eV).

In this paper, we used, for the first time, a hybrid method instead of the Hubbard model to simulate the effects of nitrogen and cobalt dual-doping in anatase. To study the synergistic effects of N and Co, both single and dual-doped TiO_2 were modeled and their data were compared. Two models of *'far'* and *'nearest neighbor'* were defined to investigate the effects of position doping on the band gap reduction. The paper is organized as follows: initially, we will provide an overview of the optimization and post-processing models. Subsequently, we will report the electronic properties of the pure perfect anatase phase with the available experimental data. Then, we will predict the electronic and optical properties of single Co- and dual (N+Co) co-doped anatase. Finally, we will summarize our conclusions.
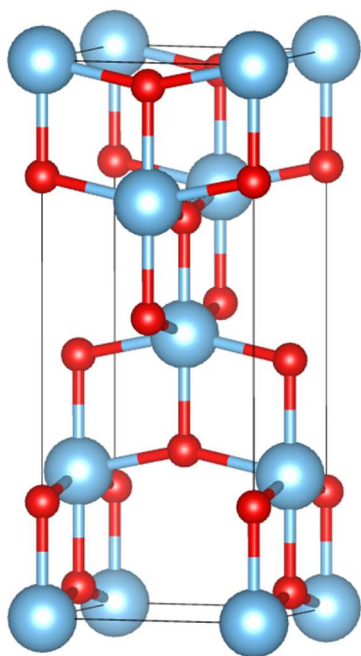
COMPUTATIONAL METHODS

The periodic DFT calculation was used to model solid-phase anatase photocatalyst. The lattice parameters and the atomic positions of a pure and doped $2\times2\times1$ supercell of anatase bulk phase were optimized during the calculations. All calculations were done by full-potential FHI-aims code [29-32]. Single and dual-doped anatase were modeled to investigate the synergistic effects between dopants on the reduction of the band gap. In the single-doped case, a Co is replaced by a Ti atom, while in the dual-doped cases, N and Co are simultaneously replaced by O and Ti atoms. The Monkhorst-Pack algorithm was used to generate a K-grid of $4\times4\times4$ to sample the first Brillouin zone [33]. The spin-collinear version of the self-consistence field method was used for all cases. Perdue-Burke-Ernzerhof (PBE) [34] and hybrid version of Perdue-Burke-Ernzerhof (PBE0) [35] methods were used for the optimization of the bulk phase and the post-processing calculations, respectively. The parameter alpha was chosen as 0.18 according to the previously used hybrid DFT works [36]. Scalar relativistic effects were included in all calculations using Zero Order Regular Approximation (ZORA). The SCF convergence criteria for energy and density were less than 10^{-5} and 10^{-4} eV, respectively. The optimization of each structure was

continued until the force on each atom was less than 0.05 eV Å^{-1}. The VESTA program was used for any graphical representation of the supercells [37].
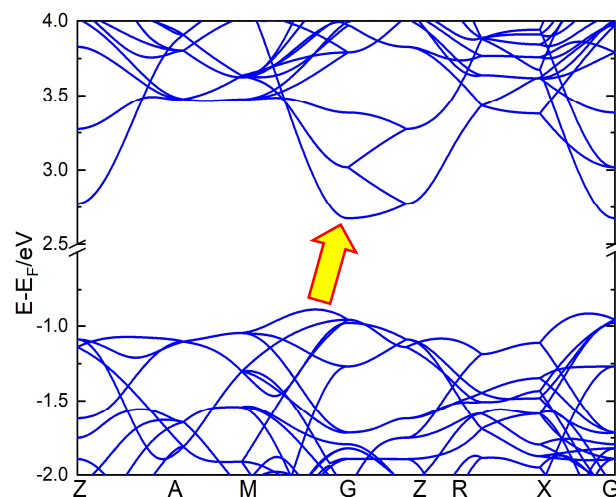
RESULTS AND DISCUSSION

Perfect Pristine Anatase Phase

The unit cell of anatase was optimized as $a = b = 3.823$ Å and $c = 9.846$ Å which deviate from the experimental data [38] by less than 3% error (Fig. 1). There are two distinct Ti-O bonds with lengths of 1.96 Å (axial bond) and 2.02 Å (equatorial bond). The calculated band gap is equal to 3.56 eV (Fig. 2), which is only +11.3% greater than the experimental value of 3.2 eV. The value of 11.3% error for the band gap is acceptable in the literature which is much less than generalized gradient approximation (GGA) methods with more than 40% error (for example, we tested PBE functional which shows 2.2 eV for the band gap of perfect pristine anatase phase). The method predicts correctly that the band gap is indirect where the valence band located between k-point M and k-point Gamma (G), and the conduction band located on the Gamma k-point (Fig. 2).
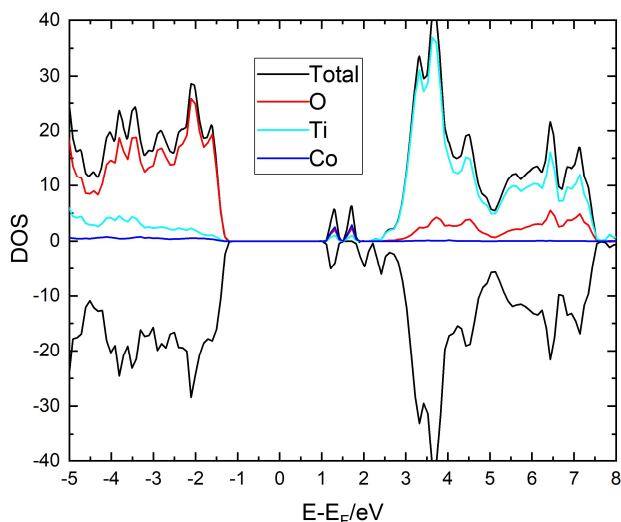

Fig. 2. Band structure for perfect pristine anatase phase. The valence band at -0.89 eV located between M and G, and the conduction band at 2.67 eV located on G. The calculated band gap is equal to 3.56 eV which is 11.3% greater than the experimental value of 3.2 eV. The Fermi level (E$_F$) is at -9.05 eV, and the band gap is indirect.

Co-doped Anatase

Cobalt is one of the transition metals that is usually used for doping TiO₂. Many experimental works used Co as a dopant for TiO₂ (For example, Ferreira et al. synthesized Co-doped TiO₂ for the degradation of triclosan [39]). Figure 3 shows the density of states (DOS) for the Co-doped anatase phase. The model shows that the band gap has been reduced by 32% from 3.56 eV to 2.40 eV. The spin magnetic moment for the studied model (Ti$_{15}$CoO$_{32}$) is equal to $1\mu_B$. This value is the same as the experimental value of Yerkamov *et al.* for a Co concentration of 4.5 at % [40]. In the model, the Co concentration is equal to 6.25 at % (Ti$_{0.9375}$Co$_{0.0625}$O₂). On the other hand, this value is the same as the magnetic moment for the Co-doped rutile phase studied by Geng and Kim [41]. Substitutional Co-doping altered the Fermi level of anatase from -9.05 eV to -8.58 eV. This means that the electrostatic interaction for Co-doped anatase is less than the perfect one and this is attributed to the changes in the charge density of Co atom which is less than the charge density of Ti atoms. The calculated Hirshfeld charges show that the Co atom has a charge of +0.39 e while the Hirshfeld charge of a Ti atom is +0.62 e.

Fig. 1. The optimized unit cell of the perfect pristine anatase. The red circles are O and the others are Ti atoms.

Fig. 3. Total and partial DOS for Co-doped anatase phase. The up-gap and down-gap are nearly the same (2.4 eV). The Fermi level is at -8.58 eV. The gap decreased by 32% compared to the perfect pristine anatase phase.

(N, Co) co-doped Anatase

Several experimental studies have been done for (N, Co) dual-doping TiO_2 [42-46]. Experiments show that N and Co have synergistic effects on the band gap reduction compared to the Co single-doped one. We modeled dual (N, Co) doped by optimizing two different supercell structures. In the first one N and Co are located far from each other, and in the second one, they are nearest neighbor. Figure 4 shows the supercells studied for this purpose. Figures 5 and 6 show DOS for these models, respectively. Data show that the band gap reduction is higher for the model in which N and Co are far from each other. The *'far'* model reduces the band gap by 44%, and the *'nearest neighbor'* model reduces it by 27%. The probability that N and Co are located in the nearest neighbor is less than the probability that they are placed far from each other. So, in many cases we will see the synergistic effects between N and Co which reduces the band gap more than the band gap reduction in the Co single-doped case; however, a situation may happen when N and Co are located nearest neighbors. In this case, N and Co show different behavior, and the band gap will be higher than the Co single-doped one. The most important factor that determines where N and Co are located is the synthesis method of doped anatase. In both models, the magnetic moments are the same and equal to $2\mu_B$. It means that the photocatalyst can be recycled by using a magnet. Figure 7 shows the absorption coefficient for the two studied *'nearest neighbor'* and *'far'* models. The figure shows that there is a small peak in the range of 300 to 600 nm. This peak shifts to the wavelengths less than 400 nm for the *'nearest neighbor'* model, while it shifts to the wavelengths higher than 400 nm for the *'far'* model.
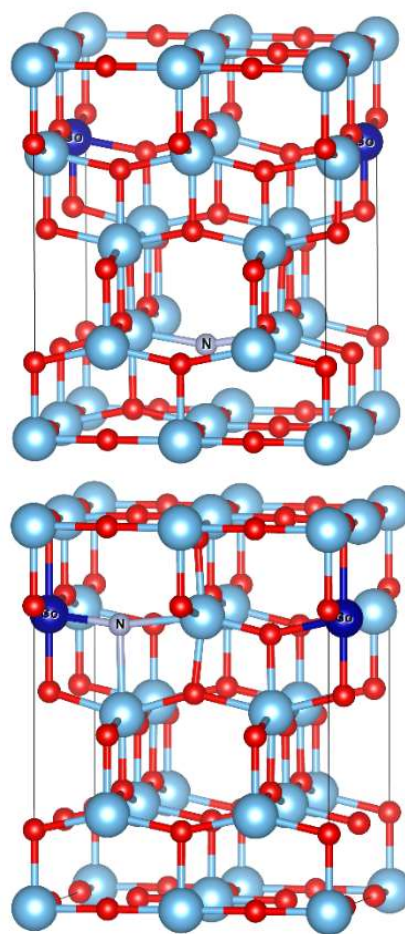

Fig. 4. The geometrical structures that were used to model (N, Co) dual-doped anatase (2×2×1) Supercell was used with the formula of $Ti_{15}CoO_{31}N$. All atoms in the boundaries have been shown. Since Co has been located in the boundary position, its periodic image has been also shown, and we see two nitrogen atoms. The up figure is for the model in which Co and N atoms are far from each other, and the down figure is for the model in which Co and N are the nearest neighbors.
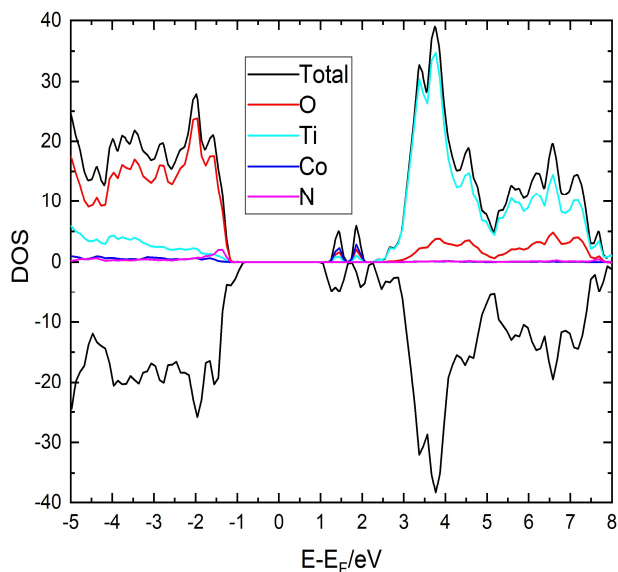
Fig. 5. Total and partial DOS for (N, Co) dual-doped *'far'* model. N and Co atoms have been located far from each other. The up-gap is 2.5 eV, and the down-gap is 2.0 eV. The Fermi level is at -8.62 eV. The down-gap decreased by 44% compared to the perfect pristine anatase phase.
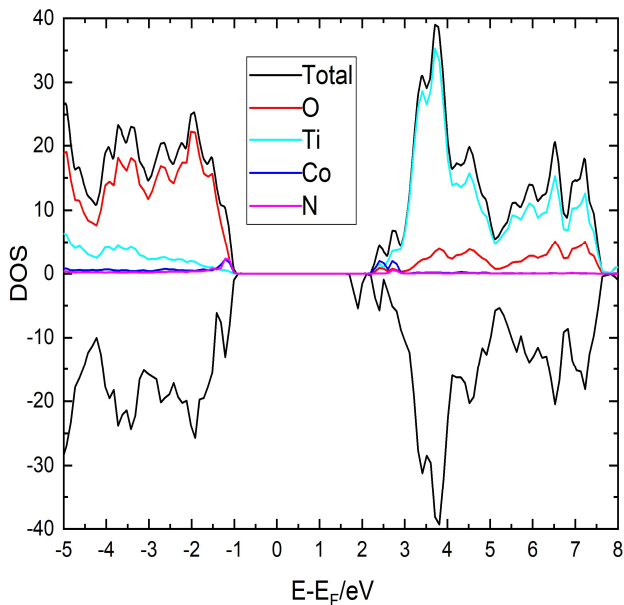
Fig. 6. Total and partial DOS for the (N, Co) dual-doped *'nearest neighbor'* model. The up-gap is 3.2 eV, and the down-gap is 2.6 eV. The Fermi level is at -8.66 eV. The down-gap decreased by 27% compared to the perfect pristine anatase phase.
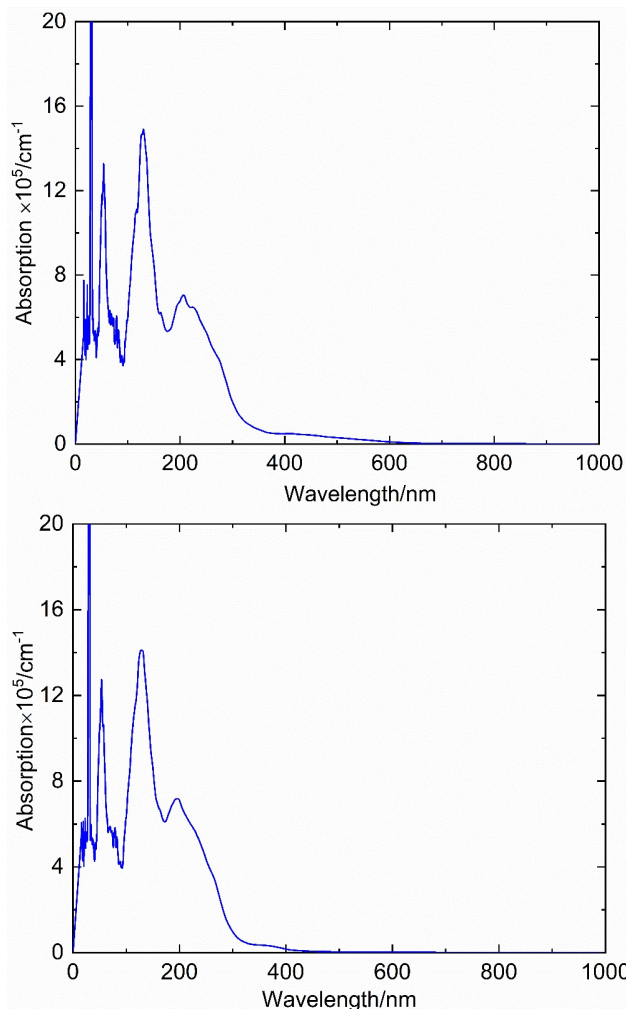
Fig. 7. Absorption coefficient for (N, Co) dual-doped anatase phase. (up): For the *'far'* model and (down): for the *'nearest neighbor'* model.

CONCLUSION

In this paper, the electronic structures of pure and doped anatase in the solid-state phase were modeled. A high-level hybrid periodic DFT method was used for the band structure and DOS calculations. Results show that the Co-doping by itself reduces the band gap from 3.56 to 2.4 eV. For the (N, Co) dual-doped case, the synergistic effects depend on the positions of N and Co dopants. If Co and N are located in the positions of the nearest neighbors, the band gap is reduced from 3.56 to 3.2 eV for spin-up, and from 3.56 to 2.6 eV for spin-down electrons, respectively. For the *'far'* model, the

band gap reduces from 3.56 to 2.5 eV for spin-up, and from 3.56 to 2.0 eV for spin-down electrons, respectively. Similar to the DOS graphs, the absorption coefficient shows that co-doping causes a small peak is formed in the visible light range. This peak shifts to the wavelengths higher than 400 nm for the 'far' model. The models predict that the synthesis method of co-doped anatase is crucial for observing the best efficiency for photocatalytic pollutant degradation. The spin magnetic moment of single and dual-doped anatase are $1\mu_B$ and $2\mu_B$, respectively, which are in line with the experimental data.

REFERENCES

[1] Bokare, A.; Pai, M. and Athawale, A. A., Surface modified Nd doped TiO_2 nanoparticles as photocatalysts in UV and solar light irradiation, *Sol. Energy*, **2013**, *91*, 111-119, https://doi.org/10.1016/j.solener.2013.02.005.

[2] Esfandfard, S. M.; Elahifard, M. R.; Behjatmanesh-Ardakani, R.; Kargar, H., DFT Study on Oxygen-Vacancy Stability in Rutile/Anatase TiO_2: Effect of Cationic Substitutions, *Phys. Chem.Res.*, **2018**, *6*, 547-563, https://doi.org/10.22036/PCR.2018.128713.1481.

[3] Sun, C.; Searles, D. J., Origin of the visible light absorption of boron/nitrogen co-doped anatase TiO_2, *The Journal of Physical Chemistry C*, **2013**, *117*, 26454-26459, https://doi.org/10.1021/jp408858u.

[4] Rashid, R.; Shafiq, I.; Iqbal, M. J.; Shabir, M.; Akhter, P.; Hamayun, M. H.; Ahmed, A.; Hussain, M., Synergistic effect of NS co-doped TiO_2 adsorbent for removal of cationic dyes, *Journal of Environmental Chemical Engineering*, **2021**, *9*, 105480, https://doi.org/10.1016/j.jece.2021.105480.

[5] Chen, H.; Li, X.; Wan, R.; Kao-Walter, S.; Lei, Y.; Leng, C., A DFT study on modification mechanism of (N,S) interstitial co-doped rutile TiO_2, *Chem. Phys. Lett.*, **2018**, *695*, 8-18, https://doi.org/10.1016/j.cplett.2018.01.044.

[6] Chen, C.; Wu, M.; Ma, C.; Song, M.; Jiang, G., Efficient Photo-Assisted Thermal Selective Oxidation of Toluene Using N-Doped TiO_2, *ACS Omega*, **2023**, *8*, 21026-21031, https://doi.org/10.1021/acsomega.3c01887.

[7] Chen, Y.; Li, A.; Fu, X.; Peng, Z., Novel F-doped carbon nanotube@(N,F)-co-doped TiO_2-δ nanocomposite: Highly active visible-light-driven photocatalysts for water decontamination, *Appl. Surf. Sci.*, **2023**, *609*, 155460, https://doi.org/10.1016/j.apsusc.2022.155460.

[8] Wang, C.; Liu, Y.; Han, H.; Wang, D.; Chen, J.; Zhang, R.; Zuo, S.; Yao, C.; Kang, J.; Gui, H., C,N co-doped TiO2 hollow nanofibers coated stainless steel meshes for oil/water separation and visible light-driven degradation of pollutants, *Scientific Reports*, **2023**, *13*, 5716, https://doi.org/10.1038/s41598-023-28992-4.

[9] Ram Kumar, A.; Selvaraj, S.; Azam, M.; Sheeja Mol, G. P.; Kanagathara, N.; Alam, M.; Jayaprakash, P., Spectroscopic, Biological, and Topological Insights on Lemonol as a Potential Anticancer Agent, *ACS Omega*, **2023**, *8*, 31548-31566, 10.1021/acsomega.3c04922.

[10] Kumar, A. R.; Ilavarasan, L.; Mol, G. P. S.; Selvaraj, S.; Azam, M.; Jayaprakash, P.; Kesavan, M.; Alam, M.; Dhanalakshmi, J.; Al-Resayes, S. I.; Ravi, A., Spectroscopic (FT-IR, FT-Raman, UV-Vis and NMR) and computational (DFT, MESP, NBO, NCI, LOL, ELF, RDG and QTAIM) profiling of 5-chloro-2-hydroxy-3-methoxybenzaldehyde: A promising antitumor agent, *J. Mol. Struct.*, **2024**, *1298*, 136974, https://doi.org/10.1016/j.molstruc.2023.136974.

[11] Behjatmanesh-Ardakani, R., Periodic hybrid-DFT study on the N-doped TiO_2 (001) nanotubes as solar water splitting catalysts: A comparison with the rutile and anatase bulk phases, *Int. J. Hydrogen Energy*, **2023**, *48*, 35584-35598, https://doi.org/10.1016/j.ijhydene.2023.05.352.

[12] Navarra, W.; Ritacco, I.; Sacco, O.; Caporaso, L.; Farnesi Camellone, M.; Venditto, V.; Vaiano, V., Density Functional Theory Study and Photocatalytic Activity of ZnO/N-Doped TiO_2 Heterojunctions, *The Journal of Physical Chemistry C*, **2022**, *126*, 7000-7011, https://doi.org/10.1021/acs.jpcc.2c00152.

[13] Keller, K.; Khramenkova, E. V.; Slabov, V.; Musin, A.; Kalashnikov, A.; Vinogradov, A. V.; Pidko, E. A., Inkjet Printing of Sc-Doped TiO_2 with Enhanced Photoactivity, *Coatings*, **2019**, *9*, 78, https://doi.org/10.3390/coatings9020078.

[14] Zhang, D. R.; Liu, H. L.; Han, S. Y.; Piao, W. X., Synthesis of Sc and V-doped TiO$_2$ nanoparticles and photodegradation of rhodamine-B, *Journal of Industrial and Engineering Chemistry*, **2013**, *19*, 1838-1844, https://doi.org/10.1016/j.jiec.2013.02.029.

[15] Hossain, M. K.; Hossain, M. M.; Akhtar, S., Studies on Synthesis, Characterization, and Photocatalytic Activity of TiO$_2$ and Cr-Doped TiO$_2$ for the Degradation of p-Chlorophenol, *ACS Omega*, **2023**, *8*, 1979-1988, https://doi.org/10.1021/acsomega.2c05107.

[16] Yen, C. -C.; Wang, D. -Y.; Chang, L. -S.; Shih, H. C., Characterization and photocatalytic activity of Fe- and N-co-deposited TiO$_2$ and first-principles study for electronic structure, *J. Solid State Chem.*, **2011**, *184*, 2053-2060, https://doi.org/10.1016/j.jssc.2011.05.036.

[17] Yin, J.; Lv, L.; Chu, Y.; Tan, L., Highly antibacterial Cu/Fe/N co-doped TiO$_2$ nanopowder under visible light, *Inorg. Chem. Commun.*, **2023**, *151*, 110587, https://doi.org/10.1016/j.inoche.2023.110587.

[18] Khan, M.; Xu, J.; Chen, N.; Cao, W., First principle calculations of the electronic and optical properties of pure and (Mo, N) co-doped anatase TiO$_2$, *J. Alloys Compd.*, **2012**, *513*, 539-545, https://doi.org/10.1016/j.jallcom.2011.11.002.

[19] Liu, Y.; Liang, W.; Zhang, W.; Zhang, J.; Han, P., First principle study of Cu/N, Cu and N-doped anatase TiO$_2$, *Solid State Commun.*, **2013**, *164*, 27-31, https://doi.org/10.1016/j.ssc.2013.04.005.

[20] Li, Z.; Wang, X.; Jia, L.; Chi, B., Synergistic effect in Fe/N co-doped anatase TiO$_2$(101) surface and the adsorption of di-, tri- and polyatomic gases: A DFT investigation, *J. Mol. Struct.*, **2014**, *1061*, 160-165, https://doi.org/10.1016/j.molstruc.2013.12.069.

[21] Yang, K.; Zhou, G., Hydrogen evolution/spillover effect of single cobalt atom on anatase TiO$_2$ from first-principles calculations, *Appl. Surf. Sci.*, **2021**, *536*, 147831, https://doi.org/10.1016/j.apsusc.2020.147831.

[22] Jensen, S.; Kilin, D., Cobalt-doped TiO$_2$: a computational analysis of dopant placement and charge transfer direction on thin film anatase, *Mol. Phys.*, **2016**, *114*, 469-483, https://doi.org/10.1080/00268976.2015.1094582.

[23] Liu, Q.; Jiang, Y.; Yan, W.; Sun, Z.; Pan, Z.; Yao, T.; Wu, Z.; Wei, S., **2009**.

[24] Weng, H.; Yang, X.; Dong, J.; Mizuseki, H.; Kawasaki, M.; Kawazoe, Y., Electronic structure and optical properties of the Co-doped anatase TiO$_2$ studied from first principles, *Physical Review B*, **2004**, *69*, 125219, https://doi.org/10.1103/PhysRevB.69.125219.

[25] Weng, H.; Dong, J.; Fukumura, T.; Kawasaki, M.; Kawazoe, Y., First principles investigation of the magnetic circular dichroism spectra of Co-doped anatase and rutile TiO$_2$, *Physical Review B*, **2006**, *73*, 121201, https://doi.org/10.1103/PhysRevB.73.121201.

[26] Janisch, R.; Spaldin, N. A., Understanding ferromagnetism in Co-doped TiO$_2$ anatase from first principles, *Physical Review B*, **2006**, *73*, 035201, https://doi.org/10.1103/PhysRevB.73.035201.

[27] Meng, Q.; Wang, T.; Liu, E.; Ma, X.; Ge, Q.; Gong, J., Understanding electronic and optical properties of anatase TiO$_2$ photocatalysts co-doped with nitrogen and transition metals, *Physical Chemistry Chemical Physics*, **2013**, *15*, 9549-9561, 10.1039/C3CP51476E.

[28] Agapito, L. A.; Curtarolo, S. and Buongiorno Nardelli, M., Reformulation of DFT+U as a Pseudohybrid Hubbard Density Functional for Accelerated Materials Discovery, *Physical Review X*, **2015**, *5*, 011006, 10.1103/PhysRevX.5.011006.

[29] Blum, V.; Gehrke, R.; Hanke, F.; Havu, P.; Havu, V.; Ren, X.; Reuter, K.; Scheffler, M., Ab initio molecular simulations with numeric atom-centered orbitals, *Comput. Phys. Commun.*, **2009**, *180*, 2175-2196, 10.1016/j.cpc.2009.06.022.

[30] Havu, V.; Blum, V.; Havu, P.; Scheffler, M., Efficient O(N) integration for all-electron electronic structure calculation using numeric basis functions, *J. Comput. Phys.*, **2009**, *228*, 8367-8379, https://doi.org/10.1016/j.jcp.2009.08.008.

[31] Marek, A.; Blum, V.; Johanni, R.; Havu, V.; Lang, B.; Auckenthaler, T.; Heinecke, A.; Bungartz, H. J.; Lederer, H., The ELPA library: scalable parallel eigenvalue solutions for electronic structure theory and computational science, *J. Phys.: Condens. Matter*, **2014**, *26*, 213201, https://doi.org/10.1088/0953-8984/26/21/213201.

[32] Yu, V. W. -Z.; Corsetti, F.; García, A.; Huhn, W. P.; Jacquelin, M.; Jia, W.; Lange, B.; Lin, L.; Lu, J.; Mi, W.; Seifitokaldani, A.; Vázquez-Mayagoitia, Á.; Yang,

C.; Yang, H.; Blum, V., ELSI: A unified software interface for Kohn-Sham electronic structure solvers, *Comput. Phys. Commun.*, **2018**, *222*, 267-285, https://doi.org/10.1016/j.cpc.2017.09.007.

[33] Monkhorst, H. J.; Pack, J. D., Special points for Brillouin-zone integrations, *Physical Review B*, **1976**, *13*, 5188-5192, 10.1103/PhysRevB.13.5188.

[34] Hammer, B.; Hansen, L. B.; Nørskov, J. K., Improved adsorption energetics within density-functional theory using revised Perdew-Burke-Ernzerhof functionals, *Physical Review B*, **1999**, *59*, 7413-7421, 10.1103/PhysRevB.59.7413.

[35] Adamo, C.; Barone, V., Toward reliable density functional methods without adjustable parameters: The PBE0 model, *The Journal of Chemical Physics*, **1999**, *110*, 6158-6170, https://doi.org/10.1063/1.478522.

[36] Kim, W. J.; Han, M. H.; Lebègue, S.; Lee, E. K.; Kim, H., Electronic Structure and Band Alignments of Various Phases of Titania Using the Self-Consistent Hybrid Density Functional and DFT+U Methods, *Front. Chem.*, **2019**, *7*, https://doi.org/10.3389/fchem.2019.00047.

[37] Momma, K.; Izumi, F., VESTA 3 for three-dimensional visualization of crystal, volumetric and morphology data, *J. Appl. Crystallogr.*, **2011**, *44*, 1272-1276, https://doi.org/10.1107/S0021889811038970.

[38] Rezaee, M.; Mousavi Khoie, S. M.; Liu, K. H., The role of brookite in mechanical activation of anatase-to-rutile transformation of nanocrystalline TiO₂: An XRD and Raman spectroscopy investigation, *CrystEngComm*, **2011**, *13*, 5055-5061, https://doi.org/10.1039/C1CE05185G.

[39] Ferreira, O.; Monteiro, O. C.; do Rego, A. M. B.; Ferraria, A. M.; Batista, M.; Santos, R.; Monteiro, S.; Freire, M.; Silva, E. R., Visible light-driven photodegradation of triclosan and antimicrobial activity against Legionella pneumophila with cobalt and nitrogen co-doped TiO₂ anatase nanoparticles, *Journal of Environmental Chemical Engineering*, **2021**, *9*, 106735, https://doi.org/10.1016/j.jece.2021.106735.

[40] Yermakov, A. Y.; Zakharova, G. S.; Uimin, M. A.; Kuznetsov, M. V.; Molochnikov, L. S.; Konev, S. F.; Konev, A. S.; Minin, A. S.; Mesilov, V. V.; Galakhov, V. R.; Volegov, A. S.; Korolyov, A. V.; Gubkin, A. F.; Murzakayev, A. M.; Svyazhin, A. D.; Melanin, K. V., Surface Magnetism of Cobalt-Doped Anatase TiO₂ Nanopowders, *The Journal of Physical Chemistry C*, **2016**, *120*, 28857-28866, https://doi.org/10.1021/acs.jpcc.6b10417.

[41] Geng, W.; Kim, K. S., Structural, electronic, and magnetic properties of a ferromagnetic semiconductor: Co-doped TiO₂ rutile, *Physical Review B*, **2003**, *68*, 125203, https://doi.org/10.1103/PhysRevB.68.125203.

[42] Song, H.; Zhou, G.; Wang, C.; Jiang, X.; Wu, C.; Li, T., Synthesis and photocatalytic activity of nanocrystalline TiO₂ co-doped with nitrogen and cobalt(II), *Res. Chem. Intermed.*, **2013**, *39*, 747-758, https://doi.org/10.1007/s11164-012-0594-x.

[43] Sharma, A.; Negi, P.; Konwar, R. J.; Kumar, H.; Verma, Y.; Shailja; Sati, P. C.; Rajyaguru, B.; Dadhich, H.; Shah, N. A.; Solanki, P. S., Tailoring of structural, optical and electrical properties of anatase TiO₂ via doping of cobalt and nitrogen ions, *Journal of Materials Science & Technology*, **2022**, *111*, 287-297, https://doi.org/10.1016/j.jmst.2021.09.014.

[44] Liu, S.; Li, Q.; Hou, C.; Feng, X.; Guan, Z., Hierarchical nitrogen and cobalt co-doped TiO₂ prepared by an interface-controlled self-aggregation process, *J. Alloys Compd.*, **2013**, *575*, 128-136, https://doi.org/10.1016/j.jallcom.2013.04.040.

[45] Song, X.; Zhou, H.; Jiang, C., Cathodic shift of onset potential on TiO₂ nanorod arrays with significantly enhanced visible light photoactivity via nitrogen/cobalt co-implantation, *Chinese Physics B*, **2021**, *30*, 058505, https://doi.org/10.1088/1674-1056/abee07.

[46] Garg, A.; Singhania, T.; Singh, A.; Sharma, S.; Rani, S.; Neogy, A.; Yadav, S. R.; Sangal, V. K.; Garg, N., Photocatalytic Degradation of Bisphenol-A using N, Co Codoped TiO₂ Catalyst under Solar Light, *Scientific Reports*, **2019**, *9*, 765, https://doi.org/10.1038/s41598-018-38358-w.